ON THE IMPORTANCE OF THE FLARE'S LATE PHASE FOR THE SOLAR EXTREME ULTRAVIOLET IRRADIANCE

THOMAS N. WOODS,[1*] FRANK EPARVIER,[1] ANDREW R. JONES,[1] RACHEL HOCK,[1] PHILLIP C. CHAMBERLIN,[2] JAMES A. KLIMCHUK,[2] LEONID DIDKOVSKY,[3] DARRELL JUDGE,[3] JOHN MARISKA,[4] SCOTT BAILEY,[5] W. KENT TOBISKA,[6] CAROLUS J. SCHRIJVER,[7] DAVID F. WEBB,[8] AND HARRY WARREN[4]

[1] Laboratory for Atmospheric and Space Physics, University of Colorado, Boulder, CO 80303, USA
[2] NASA Goddard Space Flight Center, Solar Physics Laboratory, Greenbelt, MD 20771, USA
[3] Space Sciences Center, University of Southern California, Los Angeles, CA 90089, USA
[4] Space Science Division, Naval Research Laboratory, Washington, DC 20375, USA
[5] Electrical and Computer Engineering Department, Virginia Tech, Blacksburg, VA 24061, USA
[6] Space Environment Technologies, Pacific Palisades, CA 90272, USA
[7] Lockheed Martin Solar and Astrophysics Laboratory, Palo Alto, CA 94304, USA
[8] Institute for Scientific Research, Boston College, Chestnut Hill, MA 02467, USA

* To whom correspondence should be addressed: E-mail: tom.woods@lasp.colorado.edu , Telephone: 1-303-492-4224

ABSTRACT

The new solar extreme ultraviolet (EUV) irradiance observations from NASA Solar Dynamics Observatory (SDO) have revealed a new class of solar flares that are referred to as "late phase" flares. These flares are characterized by the hot 2-5 MK coronal emissions (e.g., Fe XVI 33.5 nm) showing large secondary peaks that appear many minutes to hours after an eruptive flare event. In contrast, the cool 0.7-1.5 MK coronal emissions (e.g., Fe IX 17.1 nm) usually dim immediately after the flare onset and do not recover until after the delayed second peak of the hot coronal emissions. We refer to this period of 1-5 hours after the flare's main phase as the late phase, and this late phase is uniquely different than long duration flares associated with 2-ribbon flares or large filament eruptions. Our analysis of the late phase flare events indicates that the late phase involves hot coronal loops near the flaring region, not directly related to the original flaring loop system but rather with the higher post-eruption fields. Another finding is that space weather applications concerning Earth's ionosphere and thermosphere need to consider these late phase flares because they can enhance the total EUV irradiance flare variation by a factor of 2 when the late phase contribution is included.

Key words: extreme ultraviolet, irradiance, solar flares

Online-only material: color figures, flare catalog, flare movie

1. INTRODUCTION

The recently launched NASA Solar Dynamics Observatory (SDO) has on board three solar instruments to study the variability and radiative output of the solar plasma with high cadence. The extreme ultraviolet (EUV) irradiance instrument, named the EUV Variability Experiment (EVE), measures the solar irradiance (full-disk radiation) and is most important for studies of Earth's atmosphere and variety of other planetary and heliophysics studies. Solar irradiance measurements also enable many studies on the variability of the solar radiation over all times scales ranging from minutes to decades and can provide calibration for some solar physics spectrographs and imagers. The high cadence (10 sec) and modest spectral resolution (0.1 nm) for SDO EVE is also valuable for examining the spectral variations during flare events. While EVE observations provide full-disk spectra, the irradiance variations during many of the flare events in 2010 have corresponded to flaring in a single active region as confirmed by examining the SDO Atmospheric Imaging Assembly (AIA) solar EUV images. The EUV spectra from EVE, EUV images from AIA, and magnetic fields from SDO Helioseismic and Magnetic Imager (HMI) are a powerful combination to study the flare processes.

The new observations by EVE are significantly improved over the current solar EUV irradiance instruments flying on the Thermosphere-Ionosphere-Mesosphere-Energetics-Dynamics (TIMED), Solar and Heliospheric Observatory (SOHO), and Geostationary Operational Environmental Satellite (GOES) spacecraft. The EVE suite includes the Multiple EUV Grating Spectrograph (MEGS) that provides EUV spectral observations with high spectral resolution of 0.1 nm from 6 to 105 nm, high cadence of 10 sec, and accuracy to better than 20%. The EUV SpectroPhotometer (ESP) provides broadband observations between 0.1 and 39 nm with even higher cadence of 0.25 sec and with improved accuracy of better than 10%. Woods et al. (2010) provide an overview of EVE's science plans, instrument design, and data products. Didkovsky et al. (2010) provide an overview of the ESP instrument and its calibration, and Hock et al. (2010) provide an overview of the MEGS instrument and its calibration. SDO was launched on 2010 February 11, and EVE began normal operations on 2010 May 1. The flare data from EVE shown here are primarily from the MEGS-A channel measuring the spectrum from 6 to 37 nm and the ESP zeroth-order channel (0.1-7 nm band) as the flare variations are most evident in these wavelengths. The EVE spectral resolution of 0.1 nm is especially significant for the wavelength range from 6 to 27 nm because previously there have only been broadband (~10 nm) EUV irradiance measurements at these wavelengths. With this resolution and also with EVE's continuous observations with 10-sec cadence, we now have a much more accurate knowledge of how the solar EUV irradiance varies during flare events.

Flares are often decomposed into an impulsive non-thermal component and a gradual (slow) thermal component that follows the impulsive phase (Donnelly 1976; Hudson 2010). The rapid

release of magnetic energy in the solar atmosphere accelerates electrons and ions during the impulsive phase, which is often dominated by intense bremsstrahlung radiation from the energetic electrons as they interact with the dense, cool plasma in the solar chromosphere and transition region. These energetic particles heat the chromosphere, and the evaporated plasma rises into the corona and emits radiation during the gradual phase. This is part of an overall process of cooling the hot plasma in progressively higher reconnecting loops (e.g., Kopp & Pneuman 1976; Svestka 1989). The gradual component normally peaks a few minutes after the impulsive phase and can usually be described as the time integral of the impulsive component, referred to as the Neupert effect (Neupert 1968). The magnetic reconnection process can be fast, so some flare models have many flaring loops, or strands within such coronal loops, heated at slightly different times to form a continuous source (Warren & Doschek 2005).

For discussing the flares, we classify them as being either compact, intermediate, or 2-ribbon and also distinguish them as being confined or eruptive flares. Flares that are primarily from a single coronal loop or occur over a small area are called compact flares. The class of 2-ribbon flares have many coronal loops crossing a long magnetic neutral line and are often associated with a large filament eruption. Long duration flares, also called Long Decay Events (LDEs) by Kahler (1977), are usually associated with this 2-ribbon flare. Many of the flares seen so far during the SDO mission do not clearly fit within these two flare classes, so we define a new class of "intermediate" flares as those that involve a small number of coronal loops over an area of about 40 Mm diameter (~1 arc-minute). Our definition of size for intermediate flares is larger than a typical compact (confined) flare (Saint-Hilaire & Benz 2002) and smaller than the 2-ribbon flares. We further subdivide these flare classes into being confined or eruptive, a distinction that has existed for a long time (Svestka & Cliver 1992). A confined flare does not have significant coronal mass leaving the flaring region, and an eruptive flare, also named as a dynamic flare by Svestka (1989), has coronal mass leaving the flaring region as seen in solar EUV and X-ray images and often also has a coronal mass ejection (CME) as seen by a white-light coronagraph. In most cases the compact flares are confined flares, and 2-ribbon flares are eruptive flares. The intermediate flare class is defined by its size and thus is not intended to imply a specific active region configuration, but most of them are eruptive flares so far during the SDO mission. As explained later, the eruptive intermediate flare class appears to be uniquely different than eruptive 2-ribbon flares.

We refer to the impulsive and gradual phases as the flare's main components and focus our report here on delayed second peaks that appear many minutes to up to five hours after the onset of the main X-ray flare. We refer to the delayed second peaks as the flare's "late phase". It is important to note that this late phase is not the delayed peaks observed in the gradual phase after the flare onset, which are associated with the cooling process of the original flaring region (e.g.,

see flare model example given by Raftery et al. 2009). When we refer to the flare's late phase, we are referencing the time period of the second peak of the Fe XVI 33.5 nm emission that occurs much after the X-ray peak and the first Fe XVI peak. As discussed later in Section 3, there are other hot coronal emissions that also exhibit this late phase. Because the Fe XVI 33.5 nm emission is the most energetic during the late phase, we choose to define the timing of the late phase based on this Fe XVI emission's behavior.

To illustrate the differences between these flare peaks, Figure 1 shows example time series of three flare classes: confined intermediate flare, eruptive intermediate flare, and eruptive 2-ribbon flare. The transition region emissions, such as the He II 30.4 nm emission (~0.08 MK), usually have their larger peak during the impulsive phase (IP) as the flare plasma heats up and will sometimes have a second smaller peak during the gradual phase (GP) as the hot flare plasma cools back down. The very hot coronal emissions, such as the Fe XX 13.3 nm emission (~16 MK), vary almost identically to the GOES X-ray (0.1-0.8 nm) time series, whose peak is used to define the boundary between the IP and GP. The Fe XX emission is on a linear scale in these plots; whereas, the GOES X-ray is plotted on a logarithmic scale. Consequently, the Fe XX and log(GOES) traces in Figure 1 appear differently from each other but are actually very similar. The cooler coronal emissions (< 5 MK) usually peak several minutes after the X-ray peak, and these delays are indicative of the cooling rate for the flaring loops. Following the cooling of the original flaring loops, the Fe XVI 33.5 nm emission sometimes shows a second increase, as in Figure 1(b), which we refer to as the late phase (LP) for those flares. Note that some flares have multiple X-ray peaks during the flare's main components (IP + GP) as that is the impulsive nature of flaring events (example is Figure 1(a)). Also note that this late phase is always long after the impulsive phase. As discussed later in Section 3, the late phase variations also appear to be uniquely different than non-flaring active region evolution, which has different spectral signatures than the late phase variations and tends to have even slower evolution than the late phase. And later in Section 5, we will discuss how this late phase is directly related to and a consequence of the continued evolution of the original flare.

It is important to note that our definition of the flare's late phase is uniquely different than a long duration flare. The physics of plasma cooling in higher loops appear to be important for both LP and LDE, but the LP has two peaks of the hot coronal emissions while the LDE has only a single gradual phase peak. More specifically, the Fe XVI 33.5 nm emission typically has its first peak delayed after the X-ray peak, and this is consistently seen for all three flares shown in Figure 1 and for most other flares too. The delay time for this first peak is a few minutes for intermediate class flares but is over an hour later for the LDE flare shown in Figure 1(c). The LP is associated with a second peak of the Fe XVI emission that is even more delayed from the X-ray peak than its first peak. The LP peak indicates a separate energy release and heating event,

but to cooler temperatures (< 5 MK) than the original flare as there is little, if any, enhancements seen in the GOES X-ray data during the LP. The LDE flares usually only have a single peak of the Fe XVI 33.5 nm emission, albeit much delayed from the X-ray peak. One could perhaps argue that this late phase is a LDE but manifested differently than the typical 2-ribbon flare that only has a single Fe XVI peak.

The frequency and importance of the late phase to the spectral irradiance has not been fully recognized until the first flare observations by SDO EVE. While there are several results for the EUV irradiance during the flare's main phase (Woods et al. 2006), previous solar EUV irradiance instruments did not have the continuous time coverage, time cadence, spectral resolution, or spectral range to adequately observe this late phase phenomenon. The preliminary studies given in Section 5 indicate that the late phase peaks are associated with coronal loops near the original flaring region, so we consider the late phase to be part of the original flare event. It is plausible that the process in eruptive (dynamic) flares and LDEs for cooling plasma from progressively higher loops (e.g., Kopp & Pneuman 1976; Svestka 1989) is the same process during the late phase, but the hot coronal emissions (namely, Fe XV and Fe XVI) manifest themselves differently for the LDE and LP flares observed so far during the SDO mission.

2. EVE FLARE OBSERVATIONS

EVE has observed 26 C-class (more common, smaller) flares and 4 M-class (moderate) flares during the first four months of normal operations starting on 1 May 2010. No large X-class flares have been observed yet during the rising phase of solar cycle 24. The flare classification is based on GOES whole Sun (or integrated) X-ray 0.1-0.8 nm measurements, which have been made for more than 30 years. The flare magnitude is defined for the X-ray peak with a letter and a number. The logarithmic letter scale uses A, B, C, M, and X for ascending orders of magnitude, and the number scale is linear. For example, a M2 flare is 20 times brighter than a C1 flare (that corresponds to a peak irradiance of 1 $\mu W/m^2$). The 21 flares with a magnitude larger than C2 are discussed here and some details of each flare are presented in the on-line appendix Table A1.

To our surprise, the Fe XV and Fe XVI emissions have large, broad delayed second peaks after many flares, being about 60% of the flares observed so far. Multiple flares within a few hours of each other complicate the identification of the delayed second peak for some flares, and some flares do not have obvious delayed second peaks. For those flares with a late phase, the delayed second peak is 40 to 300 minutes after the main flare peak; the average delay is 140 minutes. The ratio of the delayed second peak to main flare peak for the Fe XVI 33.5 nm emission ranges from 0.3 to 2.9; the average ratio is 0.9.

The hot coronal emissions with formation temperature near 3 MK, such as the Fe XVI 33.5 nm emission, exhibit this delayed second peak phenomenon the best. The time series of

cool, moderate, and hot coronal emissions are shown in Figure 2(a) for the Fe IX 17.1 nm (~0.7 MK), Fe XII 19.5 nm (~1.4 MK), and Fe XVI 33.5 nm (~2.7 MK) emissions, respectively. As the EUV emissions have very different quiet Sun magnitudes, the irradiance changes shown in Figure 2 are relative to the emission minimum during that day. For those emissions shown in Figure 2(a), the Fe XVI emission shows the strongest variation during the flare's main phase as indicated by vertical dotted lines for the C2.3, C8.8, and M1.2 flares that occurred on 2010 May 5.

Following the flare event, the Fe XVI emission decreases, similar to the GOES X-Ray Sensor (XRS), but then slowly increases with a delayed second peak 0.5 to 5.5 hours after the main flare peak. In contrast, the cooler Fe IX emission usually dims immediately after the flare events and begins to recover at about the time of the delayed second peak of the Fe XVI emission. The Fe XII emission shows less variability but has some of the same characteristics as the other two emissions by dimming after the flare event and having a small delayed second peak a few hours later. It is interesting to note that a cooling trend is often seen in this set of emissions, namely a peak of the hot Fe XVI emission is followed by a peak of the moderate Fe XII emission, and then followed by a peak of the cool Fe IX emission.

There are hundreds of other emission lines in the EUV spectra with many being blends for EVE's 0.1 nm spectral resolution, but the five emission lines selected for Figure 2 represent reasonably well how the other EUV emission lines behave. In particular, the cool coronal Fe IX, Fe X, and Fe XI emissions vary similarly; the moderately warm coronal Fe XII, Fe XIII, and Fe XIV emissions vary about the same, and the hot coronal Fe XV and Fe XVI emissions have similar variations. Both the much cooler transition region emissions such as the He II 30.4 nm (~0.08 MK) and very hot coronal emissions Fe XX 13.3 nm (~16 MK) emissions, shown in Figure 2(b), exhibit their largest increases during the flare's main phase, as do the X-ray measurements, but no significant variations after the flare main phase. The log of the GOES X-ray emission is also included in Figure 2(b) as it has sometimes been used as a proxy for the short-term variations of the solar EUV irradiance (e.g., Chamberlin et al. 2008). We note that the GOES X-ray emission correlates well with the very hot coronal emissions and that the time derivative of the GOES X-rays (Neupert effect) correlates reasonably well with the transition region emissions. But, the GOES X-ray emission in either form does not correlate well with the multi-hour variations seen in the other coronal emission lines (~0.7 to 3 MK), so new studies for how to best model the coronal emissions are required.

As another surprise, some 80% of the C-class flares in our study are associated with CMEs. Earlier studies revealed what appeared to be a steady increase in the fraction of CME-related events as a function of flare magnitude, ranging from ~20% for C flares, to ~40% for M flares, and reaching close to ~100% for X flares (Andrews 2003; Wang & Zhang 2007; Yashiro et al.

2005). One difference between our sample and the data studied by the above references is that the Sun in 2010 was still very inactive, with few active regions and no large ones, while the earlier studies were based on events during the rise and maximum phases of the solar cycle.

3. LATE PHASE CATEGORIES

The spectral variations during these flares are similar during the flare's main phase but have differences during the late phase that are dependent on the flare type. From comparing the EVE and GOES X-ray measurements and examining solar EUV images made by the SDO Atmospheric Imaging Assembly (AIA), we have identified four categories of the delayed second peaks during the flare's late phase. However, these EVE flare observations are just of smaller flares ranging from C2 to M2; thus very different spectral variations could exist for larger flare events. Example time series of the four different Late Phase (LP) categories are provided in Figure 3.

The LP Category 1 flares have large delayed second peaks for the Fe XV and Fe XVI emissions and there are no significant X-ray flares during the second peak. Another identifying feature for the LP-1 category is that the X-ray data clearly have a change in slope on a logarithmic scale during the delayed second peak. As indicated in Figure 4, the LP-1 flares are associated with eruptive intermediate flares. So far, 50% of the eruptive intermediate flares during the SDO mission have had this type of late phase behavior.

The C8.8 and M1.2 flares on 2010 May 5, shown in Figure 2, are examples of LP-1 flares. A close up of the C8.8 flare time series is also shown in Figure 3. The spectral variations from the MEGS A channel (6-37 nm) for this C8.8 flare are provided in Figure 5 and are shown as the irradiance change relative to the pre-flare irradiance spectrum. The time at the peak of the GOES 0.1-0.8 nm irradiance is chosen to represent the flare main component, and therefore shows the gradual phase variation. The peak time of the Fe XVI 33.5 nm emission is chosen to represent the late phase variation. The most variable emissions during the main flare peak are the hot and very hot coronal lines in the 9 to 15 nm and 25 to 37 nm ranges, and they are consistently detected in all EVE flare observations. While the transition region He II 30.4 nm emission shows only a small percent of variation during the flare, it does have a large absolute energy variation due to it being the brightest solar line in this EUV range. The interpretation of the He II 30.4 nm variability is somewhat complicated by a blend with the coronal Si XI 30.33 nm emission.

The late phase spectral variations are also shown in Figure 5 for the C8.8 flare. These variations are usually less than the main phase variations but are still important as the delayed second peaks can persist for several hours. The delayed second peak variations, relative to the pre-flare spectrum, are typically dominated by the hot coronal Fe XV and Fe XVI emission lines.

Some of the brighter Fe XV emissions are at 24.4, 25.7, and 28.4 nm, and the brighter Fe XVI emissions are at 25.1, 26.3, 33.5, and 36.1 nm.

The late phase variations are spectrally different than active region evolution as the example comparison indicates in Figure 6. The active region evolution on 2010 May 13, a day when there were only small flares, indicates a more spectrally flat variation than the late phase variation that is dominated by Fe XV and Fe XVI enhancements. This active region evolution is over a 10-hour period and is one of the largest found so far during the SDO mission. Several non-flaring periods were examined, and they indicate similar spectral variations, namely most emissions increasing and decreasing together. There is some thermal evolution for the active regions as sometimes the cool coronal emissions dim or brighten out of phase with the hot coronal emissions. Furthermore, these active region variations are much less pronounced than the late phase variation that have strong brightening of the Fe XV and Fe XVI hot coronal emissions.

As illustrated in Figures 2 and 3, the cool coronal Fe IX 17.1 nm emission has dimming soon after the flare onset. The Fe X and Fe XI emissions also show dimming but the Fe IX emission usually has the largest decrease after the flare event. The recovery of these cool coronal emissions typically begins near the time of the delayed second peak of the hot coronal emissions. Coronal dimming is associated with CMEs (Rust 1983; McIntosh et al. 2007), and Aschwanden et al. (2009) even relates the amount of the EUV dimming to the mass loss in the CME. The magnitude of the Fe IX dimming in the EVE irradiance measurement is correlated ($R \sim 0.7$) with both CME width (as proxy for CME mass) and CME velocity. The parameters of the CMEs associated with these flares are also provided in Table A1. The duration of the coronal dimming can be a few hours to a day or so (Rust 1983; Sterling & Hudson 1997; Reinard & Biesecker 2008). The high correlation for our LP-1 flares having both dimming of the cool coronal emissions and delayed second peak of the hot coronal emissions suggests that the eruption process in an intermediate flare may be the cause for both phenomena.

The LP Category 2 flares have large delayed second peaks for the Fe XV and Fe XVI emissions much like the LP-1 flares, but there are several smaller X-ray flares from the original flaring region during the second peak. This delayed second peak is broad though and does not always have the narrow peaks in sync with the small X-ray flare peaks. It is not clear if the secondary flares are even playing a key role in the LP-2 delayed second peaks; however, the heating mechanism may not be the same process, or at least not as energetic as the original main flare event. The Fe XV and Fe XVI delayed second peaks for LP-2 flares appear similar to the LP-1 flares, but a distinguishing difference is that the delay of the second peak from the main flare peak is about 220 minutes (± 60 minutes) for Category 2 versus about 70 minutes (± 20 minutes) for Category 1. The C2.3 flare on 2010 May 5, as shown in Figure 3, is an example of a LP-2 flare. As indicated in Figure 4, the LP-2 flares are also associated with eruptive

intermediate flares. So far, 40% of the eruptive intermediate flares during the SDO mission have this type of late phase behavior. Because both LP Categories 1 and 2 are exclusively seen for eruptive intermediate flares, it is possible that the late phase processes are the same for LP Categories 1 and 2 but that manifestation of small X-ray flares is slightly different between Categories 1 and 2.

The LP Category 3 flares have large second peaks for the Fe XV and Fe XVI emissions but these peaks are directly related to having two or more peaks in the X-ray irradiance of similar magnitude. In other words, the Category 3 is a false detection of a real late phase component. The C2.0 flare on 2010 May 7, as shown in Figure 3, is an example of a Category 3 flare. The Fe XVI second peak is larger than the main flare peak and is delayed several minutes after the X-ray flare peak.

There are also several flares that do not have a late phase. That is, there is no obvious delayed second peak of the Fe XV and Fe XVI emissions. The majority of these flares without a LP are 2-ribbon flares. These flares are also considered to be long duration events (LDEs) as the X-ray and EUV irradiances have a slow decay over several hours. The C3.2 flare on 2010 August 1 is an example of a flare without a late phase, and its time series is shown in Figure 3. The Fe XVI emission only has a single peak; however, its peak is about an hour later than the X-ray peak. The delay of the main phase Fe XVI peak relative to the X-ray peak is also seen in the other flares, but this delay is more obvious for the 2-ribbon flares.

The LP-3 flares and flares without a late phase are not discussed further here. The geoeffectiveness and the solar process for the LP Categories 1 and 2 flares are briefly discussed in the next two sections.

4. LATE PHASE GEOEFFECTIVENESS

The irradiance integrated shortward of 45 nm is an important indicator for the solar EUV irradiance input to Earth's ionosphere and thermosphere. Strickland et al. (1995) defined this 0 to 45 nm EUV band as the Q_{EUV} and is part of their analysis of Earth's far ultraviolet (FUV) airglow. Then further integration over time provides the total flare energy in the Q_{EUV} band. This total energy of the delayed second peak exceeds the main flare peak energy for 40% of the LP Categories 1 and 2 cases due to the hot coronal emissions having a large, broad second peak. The amount of the Q_{EUV} energy released during the late phase relative to the initial X-ray flare energy ranges from 0.3 to 2.4, with average value of 1.2. In other words, there is typically twice as much energy from this type of flare when including its late phase contribution. For the example C5.7 flare shown in Figure 7, the Q_{EUV} has a 13.9% increase at the main flare peak and a 1.8% increase at its delayed second peak 63 minutes later, both of these increases are relative to its pre-flare value. Furthermore, the relative Q_{EUV} integrated over the main phase and late phase has

energy flux of 0.12 J/m^2 and 0.15 J/m^2, respectively. Although the late phase Q_{EUV} peak is much smaller than the main phase peak, the late phase duration is much longer and consequently the late phase energy is larger than the main phase energy change of the Q_{EUV}.

For 20% of the late phase flare cases, the cool coronal emissions have large dimmings and consequently the Q_{EUV} total energy change during the delayed second peak is negative relative to the main flare peak energy. For these cases, the Q_{EUV} energy change is 30% less when the late phase contribution is included. Because the GOES XRS measurements only capture the flare's main components well, current empirical flare-irradiance models, such as Flare Irradiance Spectral Model (FISM) (Chamberlin et al. 2008) and Solar Irradiance Platform (SIP) (Tobiska et al. 2000) that use the emission measured by the XRS as a flare proxy, are improperly estimating the total flare energy. Obviously, new flare models need to be developed with the EVE data for the space weather community.

With the new EVE data set, we can address which spectral features are contributing the most to the Q_{EUV} band. It is important to note that during non-flaring times the Q_{EUV} is dominated by the very bright He II 30.4 nm emission and the many bright Fe emissions in the 17 to 21 nm range (see Figure 5(a)). Figure 7 shows the Q_{EUV} near the time of the C5.7 flare on 2010 May 1 and decomposition of the Q_{EUV} into broad bands. The 0-7 nm band is from the ESP zeroth-order channel. The 7-17 nm, 17-27 nm, and 27-37 nm bands are the irradiances integrated over wavelength using MEGS-A spectra. The 37-45 nm band is the integrated irradiance using MEGS-B spectra. To highlight the flare (short-term) variations, the Q_{EUV} irradiance variations in Figure 7 are relative to the Q_{EUV} pre-flare minimum. The most obvious contribution to the Q_{EUV} variation is the 0-7 nm band during the flare's main peak, and next most important main flare contribution is the 7-17 nm band. The delayed second peak seen so clearly in the hot coronal emissions is not very apparent in the Q_{EUV} time series. However, the Q_{EUV} after the flare event is elevated relative to the pre-flare level, and the 27-37 nm band is most responsible for this elevated Q_{EUV} level.

The impact of the solar EUV irradiance on Earth's atmosphere is highly dependent on the spectral variations. For example, the solar 0-7 nm irradiance is deposited lower in the ionosphere and thus the main flare event is most effective in the lower ionosphere. However, the solar 27-37 nm is absorbed higher in the ionosphere and thermosphere, thus the long duration of the delayed second peak in the EUV irradiance will have a larger impact on the upper layers of the ionosphere and thermosphere and for over a longer period than the short burst of EUV energy from the main flare event.

5. LATE PHASE PROCESSES

Detailed analysis of solar images, primarily of SDO's Atmospheric Imager Assembly (AIA) solar EUV images, can provide insight into the evolution of the flare events and possible causes of the delayed second peaks that we see in the solar EUV irradiance time series. One enlightening technique is to view difference images — the difference of one solar image from an image taken a few minutes before. Another useful technique is examining the time series of the signal from small regions near the flare event. It is challenging to highlight the similarities or differences with every flare observed so far by SDO, so for this paper we concentrate on the C8.8 flare on 2010 May 5. We provide some AIA images and additional time series plots for this flare event in Figures 8 and 9 and also include a movie of this flare as on-line material. Figure 8 highlights four times during the flare evolution, pre-flare, main flare peak, late phase peak, and post late phase peak. The top panel in Figure 9 highlights the flare evolution of the main flare region and upper loops region that is responsible for the late phase peak. These two regions, shown in bottom right image of Figure 8, account for more than 85% of the flare variations. The bottom panel of Figure 9 shows the EVE irradiance time series, including the EVE spectra convolved to the AIA 335 band. Note that the AIA-335 variability is scaled down in Figure 9(b), as expected from the EVE data being from the full disk while the AIA signal is from just the 500 x 500 pixel active region. This effect could explain some of the differences between the EVE-derived AIA-335 band and measured AIA-335 signal, and perhaps the broad band nature of the AIA 335 band also contributes to these differences.

This C8.8 flare was from active region (AR) 11069, which was located at 40° W and 41° N on the solar disk. AR 11069 is a complex multi-polar active region and is the site for 6 of the 8 LP Category 1 and 2 flares. The central, lower part of the region clearly erupts as seen in the AIA movies. Upward motions are visible as early as 11:16 UTC, but rapid acceleration commences at about 11:49 UTC. It is at this time that a classic flare loop arcade first appears. The arcade has a bright cusp-shaped top and slowly grows as more and more reconnected magnetic flux accumulates. The magnetic reconnection that powers the main peak emission is an intimate part of the eruption process. It begins early in the event, when the erupting structure is still well within the AIA field of view. While the onset of the eruption may be due to what is known as breakout reconnection (Antiochos et al. 1999), it is the flare reconnection that produces the rapid acceleration (MacNeice et al. 2004).

We propose that the delayed second peak may have a similar physical origin, but that the location and rate of reconnection are much different. This later reconnection is thought to be more a consequence of the eruption than it is a cause. It involves magnetic fields that arch high over the active region in the pre-eruption state, in contrast to the low-lying core fields that are involved in the main phase reconnection. The eruption stretches open these initially closed

magnetic fields to create a vertical current sheet. Reconnection at high altitudes in the sheet reforms the closed fields by producing new loops that accumulate, one on top of the other. The active region is essentially rebuilt from the bottom up, though with less shear and less stress than the original pre-eruption state. The loops cool as they accumulate and therefore hot loops are observed to overlie cooler loops in the AIA images. Furthermore, emissions near 3 MK, such as from Fe XV and Fe XVI, tend to be more diffuse because the rate of cooling is relatively slow at these temperatures and many overlapping loops are visible at the same time. Distinct loops are more evident in emissions near 1 MK, such as from Fe IX, because the cooling is faster and fewer loops are present at once (Patsourakos et al. 2002; Guarrasi et al. 2010).

Long-duration emission following flares has been previously observed (McKenzie & Hudson 1999; Gallagher et al. 2002). It is well known that many large eruptive flares, primarily from 2-ribbon flares, have a GOES X-ray signal that can persist for several hours. What is new is the realization that many additional flares, namely the eruptive intermediate flares, have long-duration emission that does not reach the 10 MK or higher temperatures where the GOES XRS is sensitive. As these new measurements suggest, it seems reasonable that the late phases of eruptive intermediate flares have weaker reconnection (less heating) than the eruptive 2-ribbon flares.

An interesting question is how often and why there is a delay before the secondary reconnection begins. Long-duration GOES XRS events, such as the August 1 flare shown in Figure 3, do not usually have such a delay in X-rays. It may be that reconnection is in fact continuous without a break, and the reason that the Fe XVI irradiance has a large dip after the main phase is that the extra emission from the reconnected loops is offset by a decrease in emission due to the evacuation of coronal material by the eruption. Such an evacuation is known to produce coronal dimmings (Rust 1983; McIntosh et al. 2007) and is very likely the reason for the decrease seen in Fe IX irradiance after the flare onset. It is worth noting that the secondary peak cannot be simply explained by the time it takes the plasma to cool from higher temperatures (Raftery et al. 2009). The observed delay is much longer than characteristic radiative and conductive cooling times, which are of order 1000 seconds.

It seems more likely that there is a delay between the main phase and late phase reconnections in this event. A possible explanation for such a delay, as well as for the weaker nature of the late phase reconnection, is that different magnetic flux systems are involved. Complex active regions, such as AR 11069, contain several topologically distinct flux systems. The fields that reconnect during the flare's main phase begin as one or more relatively compact, high field strength structures in the core of the active region. We know this because the footpoints of the flare arcade are not widely separated. The fields that reconnect during the late phase are weaker and larger-scale fields that span the entire active region. The Fe IX and Fe XVI

loops produced during the late phase are high arching and have footpoints located near the active region perimeter. These differences may explain both the timing and intensity differences of the two phases. We speculate that a true late phase (as opposed to a late phase that is an artifact of coronal dimming) requires the eruption of a complex multi-polar active region. Our quick analysis of HMI magnetograms and AIA movies seems to bear this out. A comprehensive study will follow.

6. CONCLUSION

Prior to the SDO EVE observations, we had not recognized the existence of the flare's late phase for the solar EUV irradiance. The delayed second peaks of the hot coronal Fe XV and Fe XVI emissions along with the GOES X-ray irradiance are used to define the late phase categories. The LP Categories 1 and 2 flares are all associated with eruptive intermediate flares. Furthermore, 80% of the eruptive intermediate flares are LP-1 or LP-2 type flares, so one could refer to the eruptive intermediate flare class as late phase flares, and vice versa.

These new EVE results are also very important for many space weather applications as deposition of the solar EUV irradiance into Earth's atmosphere depends on the spectral variability, that is which wavelengths are varying, and on the timing that determines the local (regional) effects on Earth. For example, the ionospheric F layer is expected to have an additional increase one to five hours after an eruptive intermediate flare due to the increase of the 25-37 nm EUV irradiance during the flare's late phase. These late phase flares are also important because they can enhance the total EUV irradiance (Q_{EUV}) flare variation by a factor of 2 when the late phase contribution is included. Our current flare irradiance models based on the GOES X-ray emission as the proxy do not predict these late phase variations, thus the new observations from SDO EVE will greatly help to improve these models.

We do not know if larger M and X-class flares will show the same behavior as these small flares observed during the beginning of the SDO mission. So far, these small flares affect the Q_{EUV} by ~2%, but the large X-class flares are expected to cause 20% to even 100% changes in the Q_{EUV} during the flare's main phase (Woods et al. 2006). Because the primary late phase results (LP Categories 1 and 2) are only from eruptive intermediate flares and not from 2-ribbon flares, we suspect that the large M and X-class flares, which are usually from 2-ribbon flares, may not have the delayed second peaks of the hot coronal emissions. As the flare processes appear to be similar for both the late phase and LDE flares, the delayed second peak of Fe XVI 3.5 nm emission seen in the late phase flares but not for the LDE flares may just be the consequence of magnetic topology and energy release differences between the smaller intermediate (late phase) flares and the larger 2-ribbon (LDE) flares. While we have made some progress in understanding the late phase solar process based on a few flares, the wealth of new

data from SDO and other solar observatories over the next several years is expected to lead to even more insightful knowledge of the solar processes during the flare's late phase.

Acknowledgments. The SDO mission and this research are supported by NASA. The authors thank Vanessa George for her assistance with this manuscript.

Supporting Online Material. The online material includes the color figures, a movie of the C8.8 flare on 2010 May 5 using the AIA 335 images, and Table A1 that list the flare observations and related results (e.g., X-ray magnitude, CMEs, coronal dimming, late phase).

REFERENCES

Andrews, M. D. 2003, Solar Phys., 218, 261

Antiochos, S. K., DeVore, R. C., & Klimchuk, J. A. 1999, Astrophys. J., 510, 485

Aschwanden, M. J., Nitta, N. V., Wuelser, J.-P., Lemen, J. R., Sandman, A., Vourlidas, & Colaninno, R. C. 2009, Astrophys. J., 706, 376

Chamberlin, P. C., Woods, T. N., & Eparvier, F. G. 2008, Space Weather J., 6, S05001

Didkovsky, L., Judge, D., Wieman, S., & Woods, T. 2010, Solar Phys., doi 10.1007/s11207-009-9485-8

Donnelly, R. F. 1976, J. Geophys. Res., 81, 4745

Gallagher, P. T., Dennis, B. R., Krucker, S., Schwartz, R. A., & Tolbert, A. K. 2002, Solar Phys., 210, 341

Garcia, H. 2000, Astrophys. J. Suppl., 127, 189

Guarrasi, M., Reale, F., & Peres, G. 2010, Astrophys. J., 719, 576

Hock, R. A., Chamberlin, P. C., Woods, T. N., Crotser, D., Eparvier, F. G., Furst, M., Woodraska, D. L., & Woods, E. C. 2010, Solar Phys., doi 10.1007/s11207-010-9520-9

Hudson, H. 2010, in Heliophysics Space Storms and Radiation: Causes and Effects, ed. C.J. Schrijver & G.L. Siscoe (Cambridge University Press, Cambridge) 123

Kahler, S. W. 1977, Astrophys. J., 214, 891

Kopp, R. A., & Pneuman, G. W. 1976, Solar Phys., 50, 85

Lean, J. L. 2005, Physics Today, June, 32

MacNeice, P., Antiochos, S. K., Phillips, A., Spicer, D. S., DeVore, C. R., & Olson, K. 2004, Astrophys. J., 614, 1028

McIntosh, S. W., Leamon, R. J., Davey, A. R., & Wills-Davey, M. J. 2007, Astrophys. J., 660, 1653.

McKenzie, D. E., & Hudson, H. S. 1999, Astrophys. J., 519, L93

Neupert, W. M. 1968, Astrophys. J., 153, L59

Patsourakos, S., Antiochos, & S. K., Klimchuk, J. A. 2002, in Proc. of the Magnetic Coupling of the Solar Atmosphere (ed. H. Sawaya-Lacoste, ESA SP-505, Noordwijk, Netherlands), 207

Raftery, C. L., Gallagher, P. T., Milligan, R. O., & Klimchuk, J. A. 2009, Astron. & Astrophys., 494, 1127

Reinard, A. A., & Biesecker, D. A. 2008, Astrophys. J., 674, 576.

Rust, D. M. 1983, Space Sci. Rev., 34, 21

Saint-Hilaire, P. & Benz, A. O. 2002, Solar Phys., 210, 287.

Solomon, S. C., Woods, T. N., Didkovsky, L. V., Emmert, J. T., & Qian, L. 2010, J. Geophys. Res., 37, L16103, doi 10.1029/2010GL044468

Strickland, D. J., Evans, J. S., & Paxton, L. J. 1995, J. Geophys. Res., 100, 12,217

Sterling, A. C., & Hudson, H. S. 1997, Astrophys. J., 491, L55

Svestka, Z. 1989, Solar Phys., 121, 399

Svestka, Z. & Cliver, E. W. 1992, in Eruptive Solar Flares, eds. Z. Svestka, B. V. Jackson, and M. E. Machado (Springer-Verlag, Berlin-New York), Lecture Notes in Physics, 399, 1

Tobiska, W. K., Woods, T. N., Eparvier, F. G., Viereck, R., Floyd, L., Bouwer, D. Rottman, G. J., & White O. R. 2000, J. Atmos and Sol. Terr. Phys., 62, 1233.

Wang, Y., & Zhang, J. 2007, Astrophys. J, 665, 1428

Warren, H. P., & Doschek, G. A. 2005, Astrophys. J., 618, L157.

Woods, T. N., Kopp, G., & Chamberlin, P. C. 2006, J. Geophys. Res., 111, A10S14.

Woods, T. N., et al. 2010, Solar Phys., doi 10.1007/s11207-009-9487-6

Yashiro, S., Gopalswamy, N., Akiyama, S., Michalek, G., & Howard, R. A. 2005, J. Geophys. Res., 110, A9

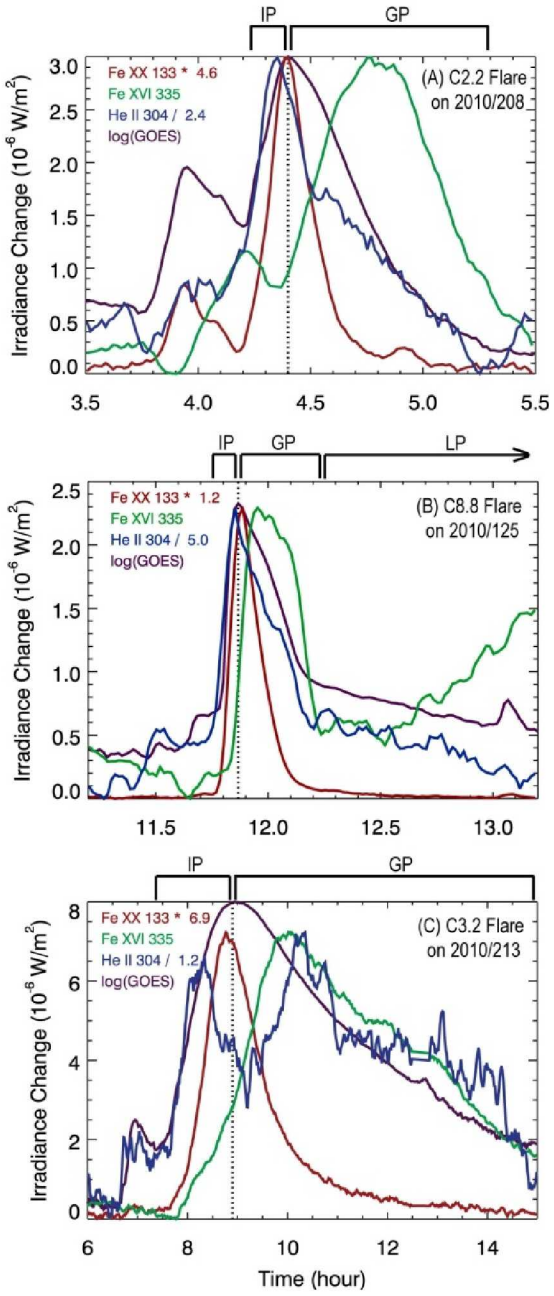

Figure 1. Example time series of (a) confined intermediate flare on 2010/208, (b) eruptive intermediate flare on 2010/125, and (c) eruptive 2-ribbon flare on 2010/213. The emissions are normalized to the Fe XVI 33.5 nm emission (~2.7 MK) to clarify the timing / phases of the flare events. The transition region emissions, such as the He II 30.4 nm emission (~0.08 MK), usually have their larger peak during the impulsive phase (IP). The very hot coronal emissions, such as the Fe XX 13.3 nm emission (~16 MK), vary much like the GOES X-ray (0.1-0.8 nm) time series, whose peak is used to define the boundary between the IP and gradual phase (GP). The cooler coronal emissions (< 5 MK) usually peak several minutes after the X-ray peak, and these delays are indicative of the cooling rate for the flaring loops. Following the cooling of the original flaring loops, the Fe XVI 33.5 nm emission sometimes shows an increase, as in panel (b), which we refer to as the late phase (LP) for those flares.

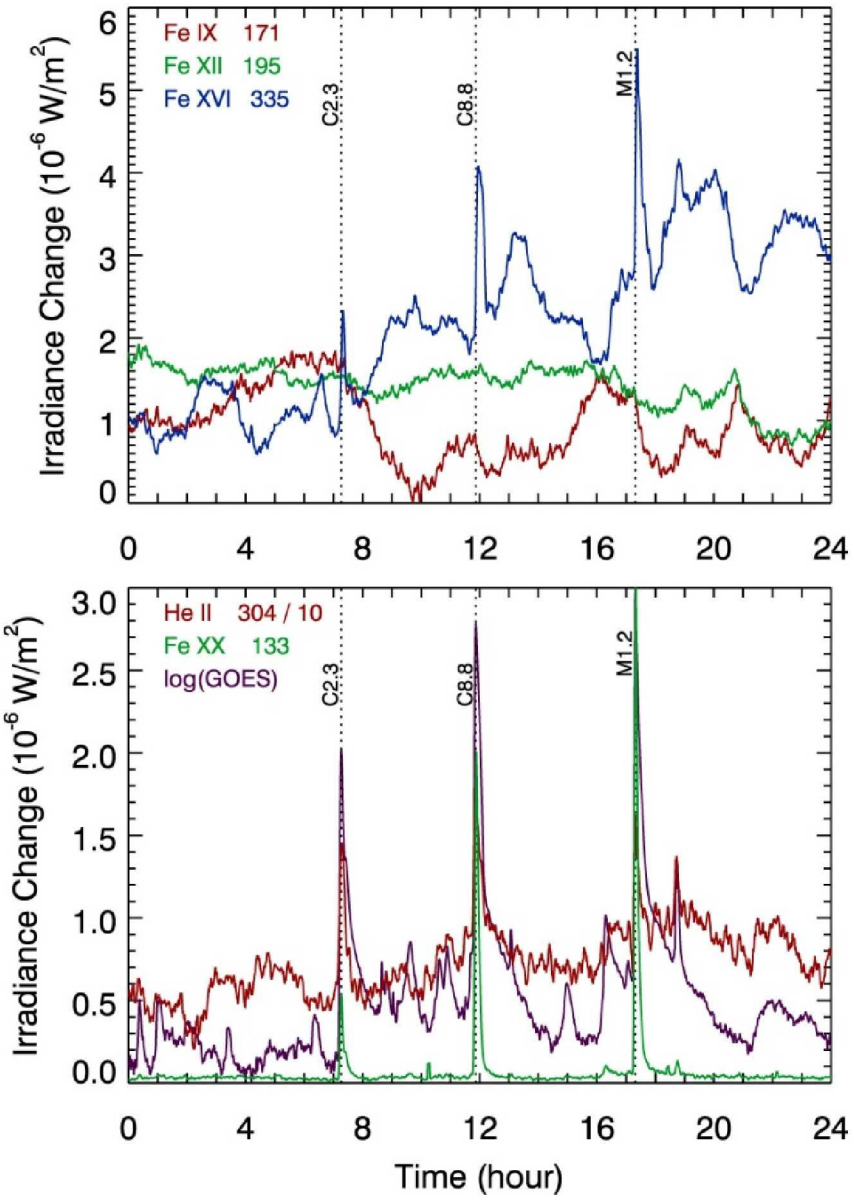

Figure 2. Times series of select EUV emissions on day 2010 May 5. Panel (a) shows the cool, moderate, and hot coronal lines of Fe IX 17.1 nm (~0.7 MK), Fe XII 19.5 nm (~1.4 MK), and Fe XVI 33.5 nm (~2.7 MK). Panel (b) has the much cooler transition region He II 30.4 nm emission (~0.08 MK), the very hot coronal Fe XX 13.3 nm emission (~16 MK), and the logarithm of the GOES X-ray 0.1-0.8 nm band. The C-class and M-class flares are indicated by the vertical dotted lines.

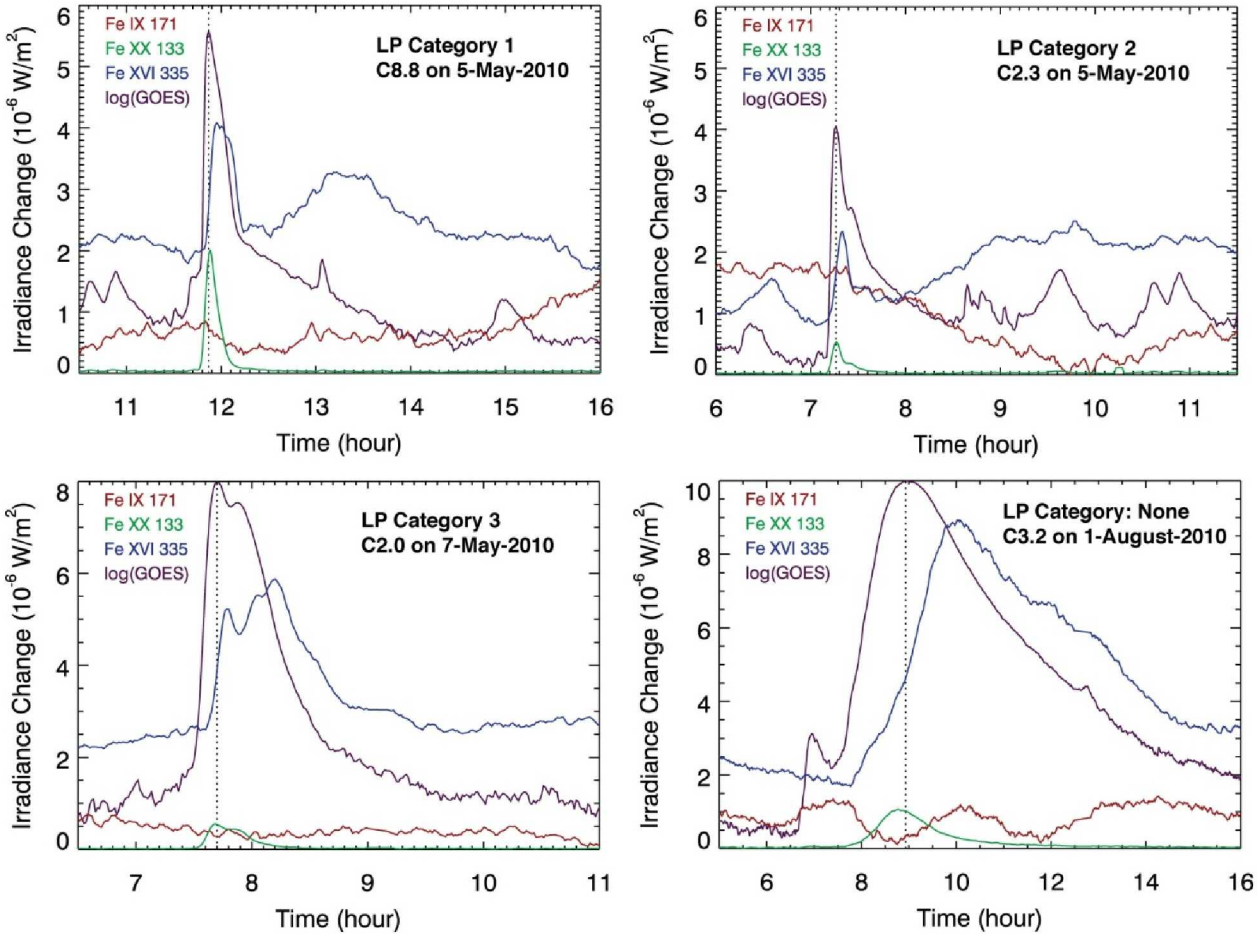

Figure 3. Examples of the Late Phase Categories. The very hot coronal Fe XX emission only has single peak in each of these examples and also behaves much like the GOES X-ray irradiance. The hot coronal Fe XVI emission has its first peak delayed from the X-ray peak and then has second peak for LP Categories 1-3. The cool coronal Fe IX emission has dimmings except for LP-3 flares. The GOES X-ray is plotted as log(GOES) and is scaled to fit the panel. The log (GOES) light curve has a notable slope change during the late phase for Category 1, and there are smaller X-ray flares during the late phase for Category 2. These examples are intermediate flares except for the 2-ribbon (long-duration) flare on 2010 August 1.

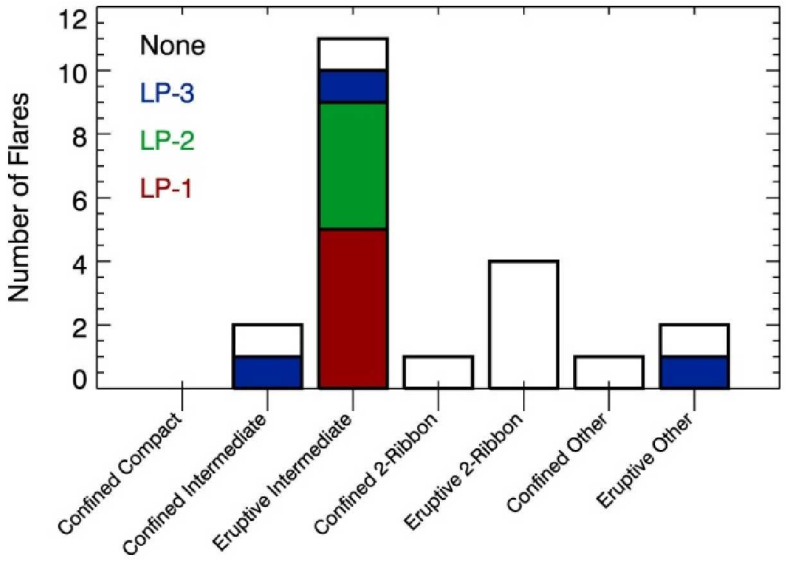

Figure 4. Late Phase Categories by Flare Type. The late phase (LP) refers to the delayed second peak of the Fe XV and Fe XVI emissions. The on-line appendix Table A1 provides the details for each flare event larger than C2 observed in May-August 2010. The "Other Flares" had poor viewing (e.g. over the limb) and thus did not clearly fit into compact, intermediate, or 2-ribbon flare type. No compact flares were identified. All 9 of the LP Categories 1 and 2 flares are eruptive intermediate flares. All of the 2-ribbon flares do not have a late phase.

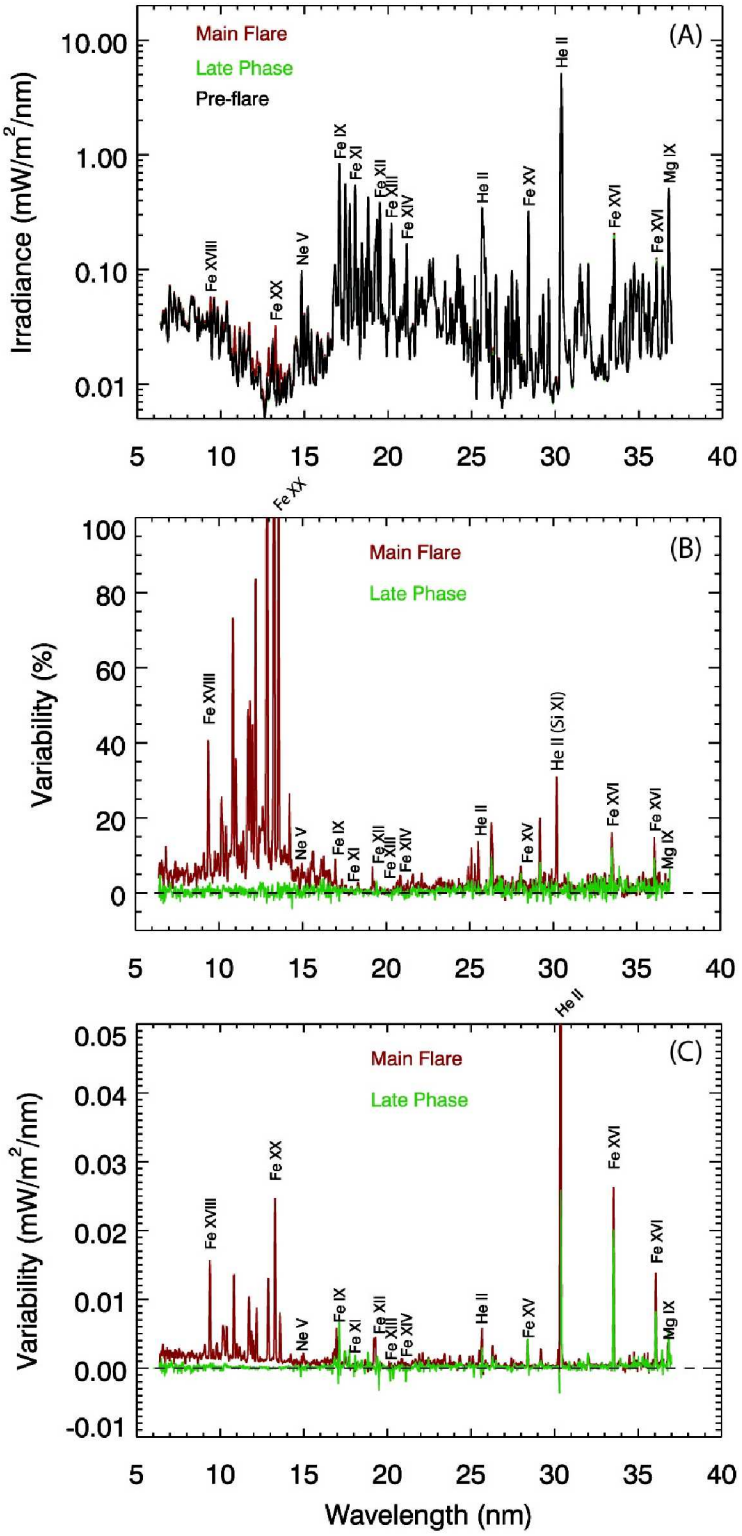

Figure 5. Flare spectral variations from the EVE MEGS A channel (6-37 nm) for the C8.8 flare on 2010 May 5. Panel (a) shows the solar spectrum, and Panels (b) and (c) show the variability during the flare's main and late phases. The variability values are relative to the pre-flare irradiance.

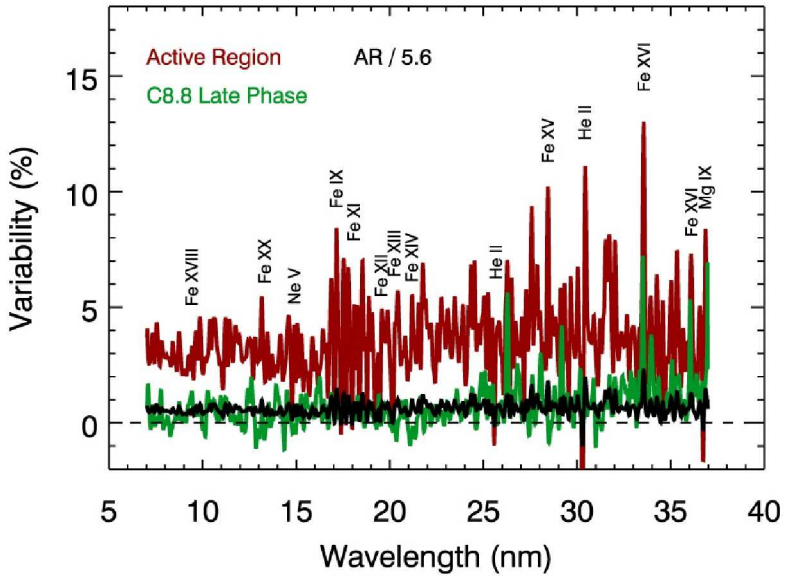

Figure 6. Spectral comparison of late phase variation to active region evolution. The late phase variation from the C8.8 flare on 2010 May 5 (green line) is compared to the active region evolution on 2010 May 13 (measured as red line and divided by 5.6 as black line for more direct comparison to LP variation).

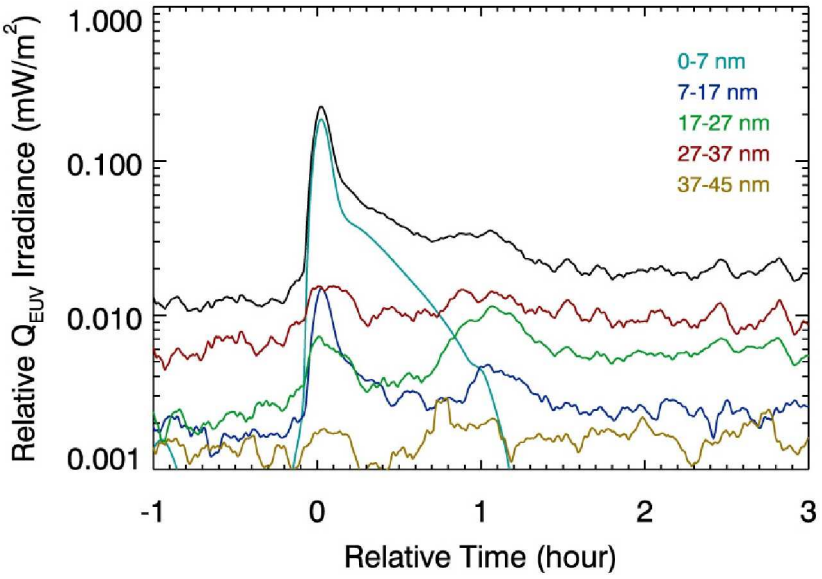

Figure 7. Time series of the EUV irradiance during the C5.7 flare on 2010 May 1. This plot shows the decomposition of the Q_{EUV} (0-45 nm) irradiance (black line) into broad bands. The relative irradiance is the change from the daily (non-flaring) minimum irradiance. The relative time is since the flare's main peak at 01:39 UT. The 0-7 nm and 7-17 nm bands dominate the Q_{EUV} during the main peak, and the 27-37 nm band dominates during non-flaring times. The late phase contributions are primarily from the 17-27 nm and 27-37 nm bands.

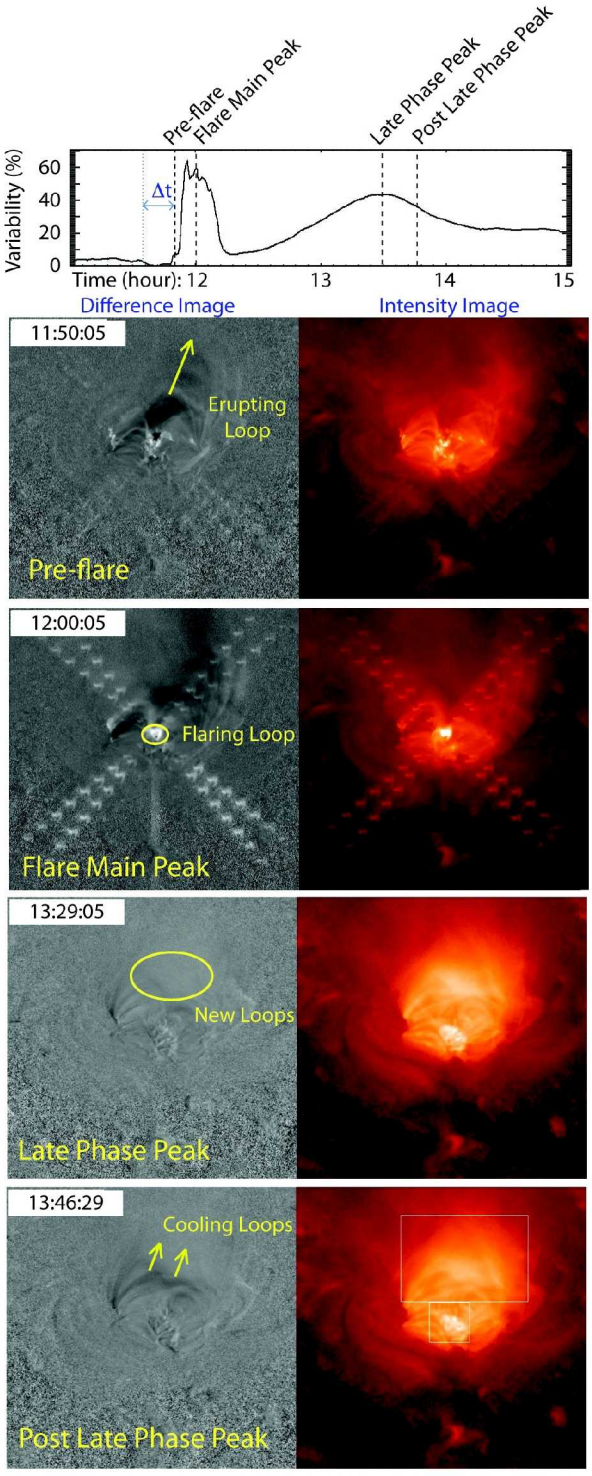

Figure 8. Time evolution of the AIA Fe XVI 33.5 nm image for active region 11069 during the C8.8 flare on 2010 May 5. The time series in the top panel is the variability of the AIA signal for this active region. The right images are the intensity images using a logarithm color scale for the intensity. The left images are the difference images by taking the difference of one image to a prior image with a time offset of Δt as shown in the time series plot. The key features of how the flare evolved are indicated on the difference images. The bottom right image includes the main flare and upper loops regions used for Figure 9.

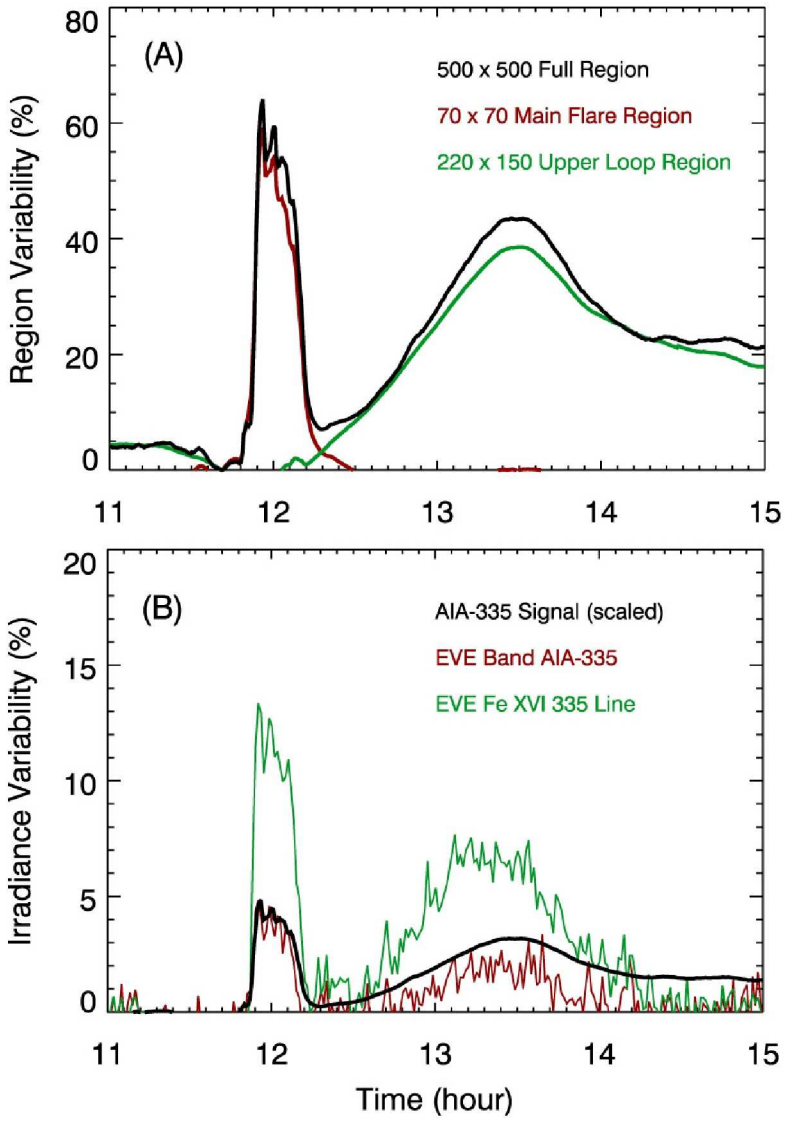

Figure 9. Time series of the C8.8 flare on 2010 May 5. Panel A shows the variability of the AIA 335 band signal for the full active region (black), main flare region (red), and upper loops region (green). These regions are shown in the bottom right image in Figure 8. Panel B shows the irradiance variability that includes the EVE Fe XVI 33.5 nm line (green), EVE spectra convolved to AIA 335 band (red), and AIA 335 band signal scaled down (black).